HHS Public Access

Author manuscript

Lab Invest. Author manuscript; available in PMC 2019 January 05.

Published in final edited form as:

Lab Invest. 2018 November ; 98(11): 1449–1464. doi:10.1038/s41374-018-0093-9.

Knockout of secretin receptor reduces biliary damage and liver fibrosis in Mdr2$^{-/-}$ mice by diminishing senescence of cholangiocytes

Tianhao Zhou[4,&], **Nan Wu**[4,&], **Fanyin Meng**[1,2,3,&], **Julie Venter**[4], **Thao K Giang**[4], **Heather Francis**[1,2,4], **Konstantina Kyritsi**[4], **Chaodong Wu**[5], **Antonio Franchitto**[6,7], **Domenico Alvaro**[8], **Marco Marzioni**[9], **Paolo Onori**[6], **Romina Mancinelli**[6], **Eugenio Gaudio**[6], **Shannon Glaser**[1,2,4,#], and **Gianfranco Alpini**[1,2,4,#]

[1]Research, Central Texas Veterans Health Care System, Baylor Scott & White Healthcare, Temple, TX 76504

[2]Baylor Scott & White Digestive Disease Research Center, Baylor Scott & White Health, Baylor Scott & White Healthcare, Temple, TX 76504

[3]Academic Research Integration, Baylor Scott & White Healthcare, Temple, TX 76504

[4]Department of Medical Physiology, Texas A&M University College of Medicine, Temple, TX 76504

[5]Department of Nutrition and Food Science, Texas A&M University, College Station, TX, 77840

[6]Department of Anatomical, Histological, Forensic Medicine and Orthopaedics Sciences, Sapienza, Rome, Italy

[7]Department of Anatomical, Histological, Forensic Medicine and Orthopaedics Sciences, Sapienza, Rome, Italy

[8]Department of Medicine, Gastroenterology, Sapienza, Rome, Italy

[9]Clinic of Gastroenterology and Hepatology, Università Politecnica delle Marche, Ospedali Riuniti - University Hospital, Ancona, Italy

Address Correspondence to Gianfranco Alpini, Ph.D., VA Research Scientist Recipient, Distinguished Professor, Medical Physiology, Director, Baylor Scott & White Digestive Diseases Research Center, Dr. Nicholas C. Hightower Centennial Chair of Gastroenterology, Central Texas Veterans Health Care System, Texas A&M Health Science Center, Olin E. Teague Medical Center, 1901 South 1st Street, Bldg. 205, 1R60, Temple, TX, 76504, Phone: 254-743-2625, Fax: 743-0555, galpini@tamu.edu, Or, Shannon Glaser, Ph.D., Associate Professor, Medical Physiology, Central Texas Veterans Health Care System, Texas A&M Health Science Center, Olin E. Teague Medical Center, 1901 South 1st Street, Bldg. 205, 1R60, Temple, TX, 76504, Phone: 254-743-2625, Fax: 254-743-0555, sglaser@medicine.tamhsc.edu.

&Drs. Zhou, Wu and Meng share the first authorship.

#Drs. Alpini and Glaser share the senior authorship.

The authors have no conflict of interest to declare.

The content is the responsibility of the author(s) alone and does not necessarily reflect the views or policies of the Department of Veterans Affairs or the United States Government.

Supplementary Information

Supplementary information is available at Laboratory Investigation's website.

Abstract

Secretin receptor (SR), only expressed by cholangiocytes, plays a key role in the regulation of biliary damage and liver fibrosis. The aim of this study was to determine the effects of genetic depletion of SR in Mdr2$^{-/-}$ mice on intrahepatic biliary mass, liver fibrosis, senescence and angiogenesis. 12 wk SR$^{-/-}$, Mdr2$^{-/-}$ and SR$^{-/-}$/Mdr2$^{-/-}$ mice with corresponding wild-type mice were used for the *in vivo* studies. Immunohistochemistry or immunofluorescence was performed in liver sections for (i) biliary expression of SR; (ii) hematoxylin and eosin; (iii) intrahepatic biliary mass by CK-19; (iv) fibrosis by Col1a1 and α-SMA; (v) senescence by SA-β-gal and p16; and (vi) angiogenesis by VEGF-A and CD31. Secretin (Sct) and TGF-β1 levels were measured in serum and cholangiocyte supernatant by ELISA. In total liver, isolated cholangiocytes or HSCs, we evaluated the expression of fibrosis markers (FN-1 and Col1a1); senescence markers (p16 and CCL2); microRNA 125b and angiogenesis markers (VEGF-A, VEGFR-2, CD31 and vWF) by immunoblots and/or *q*PCR. *In vitro*, we measured the paracrine effect of cholangiocyte supernatant on the expression of senescent and fibrosis markers in human hepatic stellate cells (HHSteCs). The increased level of ductular reaction, fibrosis and angiogenesis in Mdr2$^{-/-}$ mice was reduced in SR$^{-/-}$/Mdr2$^{-/-}$ mice. Enhanced senescence levels in cholangiocytes from Mdr2$^{-/-}$ mice were reversed to normal in SR$^{-/-}$/Mdr2$^{-/-}$ mice. However, senescence was decreased in HSCs from Mdr2$^{-/-}$ mice but returned to normal values in SR$^{-/-}$/Mdr2$^{-/-}$ mice. *In vitro* treatment of HHSteCs with supernatant from cholangiocyte lacking SR (containing lower biliary levels of Sct-dependent TGF-β1) have decreased fibrotic reaction and increased cellular senescence. Sct-induced TGF-β1 secretion was mediated by microRNA 125b. Our data suggest that differential modulation of angiogenesis-dependent senescence of cholangiocytes and HSCs may be important for the treatment of liver fibrosis in cholangiopathies.

Introduction

In addition to playing a role in the modification of the composition of canalicular bile before reaching the small intestine[1], cholangiocytes are the target cells in a number of chronic cholestatic liver diseases including primary sclerosing cholangitis (PSC) and primary biliary cholangitis (PBC)[2–5]. With the absence of effective treatment, PSC patients are likely to develop into cholangiocarcinoma (CCA)[3, 6].

Proliferating cholangiocytes secrete and respond to neuroendocrine hormones including secretin (Sct)[7, 8], which is secreted by S cells of the duodenum, as well as cholangiocytes[9]. In addition to stimulating biliary bicarbonate secretion by interaction with basolateral receptors (SR) expressed only by cholangiocytes[7, 10–12], the Sct/SR axis plays a key role in the modulation of biliary mass and liver fibrosis by both autocrine/paracrine mechanisms[2, 8, 9]. For example, the activation of the Sct/SR axis increases: (i) intrahepatic biliary mass by microRNA 125b-dependent increased expression of vascular endothelial growth factor-A (VEGF-A)[9]; and (ii) liver fibrosis by enhanced secretion of biliary transforming growth factor-β1 (TGF-β1) leading to paracrine activation of hepatic stellate cells (HSCs)[2, 9]. Conversely, knockout of SR or administration of a SR antagonist (Sct 5–27) inhibits ductular reaction and ameliorates liver fibrosis in bile duct ligated and Mdr2$^{-/-}$ mice[2, 8, 9]. Furthermore, enhanced expression of the Sct/SR/TGF-β1 axis has been demonstrated in the liver of PSC patients compared to healthy individuals[2].

Cellular senescence is a cell cycle arrest of proliferation that occurs when cells experience cellular stress, including DNA damage, dysfunctional telomeres and oncogenic mutations[13]. Cellular senescence of cholangiocytes and its associated secretion of senescence-associated secretory phenotypes (SASP, e.g., TGF-β1, p16, CCL2 and SA-β-gal)[2, 14] is a key hallmark of cholangiopathies including PSC and PBC, which contributes to the paracrine activation of HSCs (coupled with decreased HSCs senescence) and enhanced liver fibrosis[15, 16]. Furthermore, in human PSC livers a large percentage of cholangiocytes exhibit SASP[15–17]. In support of this concept, we have previously shown that: (i) substance P-induced increase in liver fibrosis is associated with enhanced biliary senescence and reduced HSCs senescence[18]; and (ii) enhanced cholangiocyte senescence (mediated by increased substance P-dependent biliary TGF-β1 secretion) leads to a paracrine activation of HSCs through decreased cellular senescence and activation of a fibrogenic phenotype[18]. However, the impact of the Sct/SR axis on the senescence of cholangiocytes and HSCs during cholestasis is unknown. In the present study, we hypothesized that the Sct/SR axis plays a regulatory role in ductular reaction and liver fibrosis through differential changes in the senescence of cholangiocytes and HSCs in the Mdr2(Abcb4) ($^{-/-}$) mouse model of PSC[2, 19, 20].

Materials and Methods

Materials

Reagents were purchased from Sigma-Aldrich Co. (St. Louis, MO) unless otherwise indicated. The RNeasy Mini Kits for RNA isolation and the selected mouse and human PCR primers were purchased from Qiagen (Valencia, CA). The mouse and human primers used are described in the Supplementary Information). The antibody for SR was obtained from Bioss (Woburn, MA). The antibodies for α-SMA, CD31, cytokeratin-19 (CK-19), Col1a1, desmin, IL-6, p16, PCNA, TNF-α, VEGF-A and VEGFR-2 were obtained from Abcam (Cambridge, MA). Enzyme-linked immunosorbent assay (ELISA) kits to measure TGF-β1 levels were purchased from Affymetrix Inc. (Santa Clara, CA). Mouse Cytokine ELISA Plate Array I to measure inflammatory cytokines was purchased from Signosis, Inc. (Santa Clara, CA).

Animal Models

The animal experiments were performed according to protocols approved by the Baylor Scott & White IACUC Committee. Male C57BL/6 wild-type (WT) mice (control for $SR^{-/-}$ mice) were purchased from Charles River (Wilmington, MA). Male FVB/NJ WT mice (25–30 gm, control for $Mdr2^{-/-}$ mice) were purchased from Jackson Laboratories (Bar Harbor, Maine). C57/FVB WT mice were obtained after breeding C57BL/6 with FVB/NJ mice. Both $SR^{-/-}$ and $Mdr2^{-/-}$ mouse colonies are established in our animal facility[2, 8]. The established mouse strains (having different backgrounds), $SR^{-/-}$ and $Mdr2^{-/-}$, were crossed until the homozygous double knockout ($SR^{-/-}/Mdr2^{-/-}$) mice were obtained. The genotype of each $SR^{-/-}/Mdr2^{-/-}$ mouse was confirmed by PCR amplification of genomic DNA extracted from the tail (described in the Supplementary Information). Animals were maintained in a temperature-controlled environment (20–22°C) with 12:12-hr light/dark cycles and fed *ad libitum* standard chow with free access to drinking water. The experiments were performed in the corresponding WT mice as well as $SR^{-/-}$, $Mdr2^{-/-}$ and $SR^{-/-}$/

Mdr2$^{-/-}$ mice (all 12 wk age) (Table 1). Before liver perfusion, animals were treated with euthasol (200–250 mg/kg BW). In all groups, we measured liver and body weight and liver to body weight ratio, an index of liver cell growth[7].

Cholangiocyte Isolation and Laser Capture Microdissection (LCM)-isolated HSCs

Cholangiocytes were obtained by immunoaffinity separation[8, 9, 11] using a monoclonal antibody (a gift from Dr. R. Faris, Brown University, Providence, RI) that is expressed by all intrahepatic cholangiocytes. Cell viability (greater than 97%) was assessed by trypan blue exclusion. HSCs were isolated by LCM[2]. Frozen liver sections (n=3, 10 μm thick) were incubated overnight with an antibody against desmin (marker of stellate cells)[21]. Following staining, desmin-positive HSCs were dissected from the slides by a LCM system Leica LMD7000 (Buffalo Grove, IL) and collected into a PCR tube before being analyzed. The RNA from HSCs was extracted with the Arcturus PicoPure RNA isolation kit (Thermo Fisher Scientific CO, Mountain View, CA). The *in vitro* studies were performed in our immortalized murine biliary cell lines (IMCLs)[9] and human hepatic stellate cell lines (HHSteCs, Sciencell, Carlsbad, USA).

SR Immunoreactivity in Liver Sections and Sct Levels in Serum and Cholangiocyte Supernatant

The immunoreactivity of SR was measured by immunohistochemistry in paraffin-embedded liver sections (4–5 μm thick, 10 different fields from 3 samples from 3 animals). Observations were processed by Image-Pro Plus software (Media Cybernetics, Silver Springs, MD) in a blinded fashion by one board-certified pathologist[22]. Sct levels were measured in serum and cholangiocyte supernatant by ELISA kits (Phoenix Pharmaceuticals, Inc., Burlingame, CA)[9].

Measurement of Liver Histology, Serum Chemistry and Intrahepatic Bile Duct Mass (IBDM)

The histology of liver, pancreas, heart, spleen, lung, kidney, stomach, small and large intestine was evaluated in paraffin-embedded liver sections (4–5 μm thick) by hematoxylin and eosin staining. Observations were processed by Image-Pro Plus software (Media Cybernetics) in a blinded fashion by a board-certified pathologist. Serum levels of glutamate pyruvate transaminases (SGPT), glutamic oxaloacetic transaminase (SGOT) and alkaline phosphatase (ALP) were measured by IDEXX Catalyst One Chemistry Analyzer and VetLab Station (Westbrook, ME). IBDM in paraffin-embedded liver sections (4–5 μm thick, 10 fields evaluated from 3 samples from 3 animals) was measured[2]. Sections were examined by the Olympus Image Pro-Analyzer software (Olympus, Tokyo, Japan). Biliary proliferation was evaluated by measurement of PCNA and Ki67 expression in cholangiocytes by immunoblots and/or *q*PCR[23]. The protocols of immunoblot and *q*PCR are described in the Supplementary Information.

Measurement of Liver Fibrosis in Liver Sections, Cholangiocytes and HSCs, and TGF-β1 Levels in Serum and Cholangiocyte Supernatant

Liver fibrosis was evaluated by Sirius Red staining in paraffin-embedded liver sections (4–5 μm thick, 10 different fields analyzed from 3 samples from 3 animals). Collagen content was

quantified by Image-Pro Plus software (Media Cybernetics, Silver Springs, MD)[22]. Immunofluorescence double staining was performed for Col1a1 (co-stained with CK-19) or α-SMA (costained with desmin) in frozen liver sections (10 μm thick). Immunofluorescent staining was visualized using Leica TCS SP5 X system (Leica Microsystems Inc.). The mRNA expression of Col1a1 and FN-1 was evaluated in cholangiocytes and/or HSCs by *q*PCR and/or immunoblots. TGF-β1 levels in serum and cholangiocyte supernatant were measured by ELISA kits[2].

Measurement of Cellular Senescence in Liver Sections, Isolated Cholangiocytes and HSCs

Biliary senescence was evaluated in frozen liver sections (10 μm thick) by staining for SA-β-gal using commercially available kits (MilliporeSigma, Billerica, MA); all the experiments were performed in 3 different liver samples from 3 animals. By immunofluorescence for p16 (co-stained with CK-19) senescence was measured in frozen liver sections (10 μm thick) for cholangiocytes. The expression of the senescent genes p16 and CCL2 were evaluated in cholangiocytes and HSCs by immunoblots and/or *q*PCR. The genes related to senescence, fibrosis and angiogenesis were analyzed using Ingenuity pathway analysis (IPA) software (Ingenuity System, Qiagen, Redwood City, CA) for the functionally relevant pathway[1, 2]. IPA is a web-based functional analysis software that helps researchers to search for targeted information on genes, proteins, chemicals, diseases, and drugs, as well as building custom biological models in life science research.

Expression of microRNA 125b, Angiogenesis and Inflammatory Genes

The expression of Sct-dependent microRNA 125b (that regulates IBDM and liver fibrosis through changes in the expression of biliary VEGF-A) was measured by *q*PCR[9]. By immunohistochemistry, we evaluated the semiquantitative immunoreactivity for VEGF-A in liver sections (4–5 μm thick, 10 different fields analyzed from 3 different samples). When 0–5% of bile ducts were positive for VEGF-A, a negative score was assigned; a +/− score was assigned when 6–10% of bile ducts were positive; a + score was assigned when 11–30% of bile ducts were positive; a ++ score was assigned with 31–60% of bile ducts positive; and a score +++ was assigned when more than 61% of bile ducts were positive. The expression of: (i) VEGF-A/R-2 in cholangiocytes and total liver; (ii) IL-6 and TNF-α in cholangiocytes; and (iii) CD31 and vWF in total liver was evaluated by immunoblots and/or *q*PCR. Immunofluorescence for the expression of CD31 was performed in frozen liver sections (10 μm thick). Immunofluorescent staining was visualized using Leica TCS SP5 X system (Leica Microsystems Inc.).

In Vitro Effect of Cholangiocyte Supernatant on the Expression of Senescent and Fibrosis Genes in HHSteCs

We performed experiments to demonstrate that cholangiocyte supernatant (displaying different levels of TGF-β1 depending on the expression of the Sct/SR axis)[2] differentially affect the expression of senescence and fibrosis of HHSteCs. In biliary supernatants, the levels of TGF-β1 were measured by ELISA kits. HHSteCs were incubated with cholangiocyte supernatants from the selected groups of animals for 12 hr (in the absence or presence of LY2109761, 10 μM, a TGF-β1 receptor antagonist, Cayman Chemical, Ann Arbor, MI)[24] before measuring the expression of VEGF-A and senescent and fibrosis genes

by *q*PCR. To determine that Sct increases TGF-β1 levels by a microRNA 125b-dependent mechanism, IMCLs were treated with Sct (10 nM in the absence/presence of a microRNA 125b mimic precursor, 5 μM)[9] for 12 hr before measuring TGF-β1 mRNA expression (by *q*PCR) and secretion by ELISA kits. To provide conclusive evidence that TGF-β1 directly modulates the function IMCLs and HHSteCs, these cells were stimulated with TGF-β1 (10 nM) for 12 hr before measuring the expression of VEGF-A and senescent and fibrosis genes by *q*PCR. IMCLs and HHSteCs were treated with r-VEGFA (100 nM)[25] for 12 hr at 37°C before measuring the expression of senescent and fibrosis markers by *q*PCR. We also evaluated by immunofluorescence the expression of VEGFR-2 in cell smears of IMCLs and HHSteCs. Immunofluorescent staining was visualized using Leica TCS SP5 X system (Leica Microsystems Inc.).

Statistical Analysis

Data are expressed as mean ± SEM. Differences between groups were analyzed by Student's unpaired t-test when two groups were analyzed and ANOVA when more than two groups were analyzed, followed by an appropriate post hoc test.

Results

Validation of the $SR^{-/-}/Mdr2^{-/-}$ Mouse Model: Expression of SR in Liver Sections

To validate SR and Mdr2 deletion in $SR^{-/-}/Mdr2^{-/-}$ homozygous mice, genomic DNA was extracted from tail and subjected to PCR genotyping analysis (Suppl. Figure 1). DNA from $SR^{-/-}/Mdr2^{-/-}$ mice showed bands corresponding to the mutant alleles of both SR and Mdr2. There was enhanced immunoreactivity of SR (red arrows) in liver sections from $Mdr2^{-/-}$ compared to the corresponding WT mice (Figure 1); no immunoreactivity for SR was observed in $SR^{-/-}$ and $SR^{-/-}/Mdr2^{-/-}$ mice compared to WT mice (Figure 1, green arrowheads).

Loss of SR in $Mdr2^{-/-}$ mice Ameliorates Liver Damage

$Mdr2^{-/-}$ mice display typical features of PSC such as increased connective tissue deposition and higher inflammatory infiltration, phenotypes that were improved in $SR^{-/-}/Mdr2^{-/-}$ mice; no significant changes were noted in $SR^{-/-}$ compared to WT mice (Suppl. Figure 2). No significant changes were observed in the morphology of pancreas, heart, kidney, stomach, small and large intestine in all animal groups (Suppl. Figure 2). The spleen of $Mdr2^{-/-}$ mice showed a higher presence of white pulp compared to red pulp, probably due to an increase in the inflammatory reaction (Suppl. Figure 2). There was enhanced inflammatory infiltration in the pulmonary parenchyma of the lungs of $Mdr2^{-/-}$ mice that was reduced in $SR^{-/-}/Mdr2^{-/-}$ mice (Suppl. Figure 2). Liver to body weight ratio increased in $Mdr2^{-/-}$ compared to the corresponding WT mice but decreased in $SR^{-/-}/Mdr2^{-/-}$ compared to $Mdr2^{-/-}$ mice (Table 1). Serum levels of SGPT, SGOT and ALP increased in $Mdr2^{-/-}$ compared to WT mice but decreased in $SR^{-/-}/Mdr2^{-/-}$ compared to $Mdr2^{-/-}$ mice (Table 1). There were enhanced TGF-β1 serum levels in $Mdr2^{-/-}$ compared to WT mice, levels that returned to values similar to that of normal values in $SR^{-/-}/Mdr2^{-/-}$ mice (Table 1).

Decreased IBDM and Liver Fibrosis in $SR^{-/-}/Mdr2^{-/-}$ Mice

In $Mdr2^{-/-}$ mice, there was increased IBDM compared to WT mice, which was reduced in $SR^{-/-}/Mdr2^{-/-}$ compared to $Mdr2^{-/-}$ mice (Figure 2 A); no significant changes in IBDM were noted in $SR^{-/-}$ compared to WT mice (Figure 2 A). There was increased expression of PCNA and Ki67 in cholangiocytes from $Mdr2^{-/-}$ mice, which was decreased in $SR^{-/-}/Mdr2^{-/-}$ compared to $Mdr2^{-/-}$ mice (Figure 2 B, Suppl. Figure 3); no significant changes were observed in the biliary expression of PCNA and Ki67 in $SR^{-/-}$ mice compared to WT mice (Figure 2 B). There was enhanced collagen deposition in liver sections from $Mdr2^{-/-}$ compared to WT mice, which was significantly decreased in $SR^{-/-}/Mdr2^{-/-}$ compared to $Mdr2^{-/-}$ mice (Figure 3 A). By immunofluorescence in liver sections, there was enhanced immunoreactivity for Col1a1 (green color costained with CK-19, red) in $Mdr2^{-/-}$ compared to WT mice, which was reduced in $SR^{-/-}/Mdr2^{-/-}$ compared to $Mdr2^{-/-}$ mice (Figure 3 B). Similarly, there was enhanced co-localization of α-SMA (red) and desmin (green) in HSCs from $Mdr2^{-/-}$ compared to WT mice, immunoreactivity that was decreased in $SR^{-/-}/Mdr2^{-/-}$ compared to $Mdr2^{-/-}$ mice (Figure 3 C). In addition, there was enhanced expression of Col1a1 and FN-1 in isolated cholangiocytes and HSCs from $Mdr2^{-/-}$ mice compared to the corresponding WT mice, increase that was significantly reduced in $SR^{-/-}/Mdr2^{-/-}$ mice compared to $Mdr2^{-/-}$ mice (Figure 3 D, Suppl. Figure 3).

Loss of SR in $Mdr2^{-/-}$ Mice Decreases Biliary Senescence but Increases Cellular Senescence of HSCs

IPA was performed to ascertain the cellular context of the differentially expressed signaling mechanisms related to the Sct/SR axis mediated liver injury. IPA analysis demonstrated that the cellular senescence pathway was the altered signaling through p16 and CCL2-related pathological mechanisms (related by the Sct/SR/micro RNA 125b/TGF-β1/VEGF-A axis) (Suppl. Fig. 4). To evaluate the underlying mechanisms by which the modulation of SR expression regulates liver fibrosis, we evaluated the effect of SR knock-out on cellular senescence in liver sections, isolated cholangiocytes and HSCs. By SA-β-gal staining in liver sections there was enhanced biliary senescence from $Mdr2^{-/-}$ compared to WT mice, which was significantly decreased in $SR^{-/-}/Mdr2^{-/-}$ when compared to $Mdr2^{-/-}$ mice (Figure 4 A). By immunofluorescence in liver sections from $Mdr2^{-/-}$ mice, there was enhanced immunoreactivity for p16 (costained with CK-19) in cholangiocytes compared to WT mice, immunoreactivity that was reduced in $SR^{-/-}/Mdr2^{-/-}$ compared to $Mdr2^{-/-}$ mice (Figure 4 B). There was enhanced expression of p16 and CCL2 in cholangiocytes from $Mdr2^{-/-}$ mice compared to WT mice, which decreased in $SR^{-/-}/Mdr2^{-/-}$ compared to $Mdr2^{-/-}$ mice (Figure 4 C, Suppl. Figure 3). Conversely, the expression of p16 and CCL2 was significantly decreased in HSCs from $Mdr2^{-/-}$ compared to WT mice, changes that returned to values similar to that of normal WT group in $SR^{-/-}/Mdr2^{-/-}$ mice (Figure 4 C).

Loss of SR in $Mdr2^{-/-}$ Mice Decreases Sct Levels, the Expression of MicroRNA 125b, Angiogenesis and Inflammatory Genes

Sct levels in serum and cholangiocyte supernatant were increased in $Mdr2^{-/-}$ mice compared to WT mice, which was decreased in $SR^{-/-}/Mdr2^{-/-}$ compared to $Mdr2^{-/-}$ mice (Figure 5 A). Consistent with our previous study[2], the expression of microRNA 125b decreased in

cholangiocytes from Mdr2$^{-/-}$ compared to WT mice, expression that returned to values similar to that of normal WT group in SR$^{-/-}$/Mdr2$^{-/-}$ mice (Figure 5 B). We also demonstrated: (i) enhanced expression of VEGF-A and VEGFR-2 in cholangiocytes and total liver as well as CD31 and vWF in total liver from Mdr2$^{-/-}$ mice compared to WT mice, changes that returned to values similar to that of normal WT group in SR$^{-/-}$/Mdr2$^{-/-}$ mice (Figures 5 B–C, Suppl. Figure 3); and (ii) increased immunoreactivity for VEGF-A and CD31 in liver sections from Mdr2$^{-/-}$ compared to relative WT mice, which was reduced in SR$^{-/-}$/Mdr2$^{-/-}$ compared to Mdr2$^{-/-}$ mice (Figures 5 D–E). Interestingly, as the Sct/SR axis also plays a key role in the paracrine regulation of liver inflammation[5, 8, 26], we observed enhanced levels of IL-6 and TNF-α in cholangiocytes from Mdr2$^{-/-}$ mice compared to relative WT mice but decreased in cholangiocytes from SR$^{-/-}$/Mdr2$^{-/-}$ compared to Mdr2$^{-/-}$ mice (Suppl. Figure 5 A). Mouse cytokine array showed increased inflammation cytokine expression in cholangiocyte supernatant from Mdr2$^{-/-}$ mice compared to WT mice, which decreased in SR$^{-/-}$/Mdr2$^{-/-}$ compared to Mdr2$^{-/-}$ mice. suggesting SR regulates inflammatory response in cholangiocytes (Suppl. Figure 5 B).

In Vitro Paracrine Effect of Cholangiocyte Supernatant on the Expression of Senescent and Fibrosis Genes in HHSteCs

There were enhanced levels of Sct-stimulated TGF-β1 in cholangiocyte supernatant from Mdr2$^{-/-}$ mice (containing higher Sct levels compared to normal cholangiocyte supernatant), levels that returned to values similar to that of relative WT group in cholangiocyte supernatant from SR$^{-/-}$/Mdr2$^{-/-}$ mice (Table 1). There was increased expression of VEGF-A and fibrotic markers but decreased senescence gene expression in HHSteCs treated with cholangiocyte supernatants from Mdr2$^{-/-}$ mice (containing higher levels of TGF-β1, Table 1) compared to HHSteCs treated with supernatant from WT mice; these changes returned to normal levels when HHSteCs were treated with cholangiocyte supernatant from SR$^{-/-}$/Mdr2$^{-/-}$ mice (Figure 6 A). These effects were also reversed when HHSteCs were preincubated with LY2109761 before treatment with the cholangiocyte supernatants from Mdr2$^{-/-}$ mice (Figure 6 B). Sct increased TGF-β1 mRNA expression of IMCLs and TGF-β1 levels in IMCLs supernatant, increases that were prevented by preincubation of IMCLs with a microRNA 125b precursor before treatment with Sct (Figure 6 C). Treatment of: (i) IMCLs with TGF-β1 and r-VEGF-A, respectively, increased the expression of VEGF-A, fibrosis and senescence genes; and (ii) HHSteCs with TGF-β1 and r-VEGF-A, respectively, increased the expression of VEGF-A, fibrosis but decreased senescence genes in HHSteCs (Figure 6 D–E). The effects of r-VEGF-A on IMCLs and HHSteCs are mediated by interaction with VEGFR-2 (Suppl. Figure 6) that is expressed in both cholangiocytes and hepatic stellate cells[25, 27].

Discussion

We demonstrated that the genetic knockout of SR in Mdr2$^{-/-}$ mice has significant inhibitory effects on ductular reaction as well as liver fibrosis through differential changes in the senescence of cholangiocytes and HSCs. The increase in biliary mass and liver fibrosis in Mdr2$^{-/-}$ mice was associated with enhanced senescence of cholangiocytes but decreased HSC senescence, changes that returned to normal values in SR$^{-/-}$/Mdr2$^{-/-}$ mice. The effects

of knockout of the Sct/SR axis in Mdr2$^{-/-}$ mice on biliary hyperplasia and liver fibrosis were associated with: (i) decreased levels of Sct and biliary Sct-dependent TGF-β1[2], which we have shown to activate biliary senescence (by an autocrine Sct-dependent loop, Wu and Alpini, unpublished observations, 2018 and Figure 6 C) and liver fibrosis by a paracrine pathway through decreased senescence of HSCs[2]; and (ii) increased biliary expression of Sct-dependent microRNA 125b[2] and subsequent reduction of microRNA 125b-dependent VEGF-A expression (that increases biliary senescence and fibrosis of IMCLs and decrease HSC senescence but increases fibrogenic activity of HHSteCs)[2]. *In vitro*: (i) Sct-induced TGF-β1 secretion was mediated by microRNA 125b; and (ii) treatment of HHSteCs with the supernatant of cholangiocyte lacking SR (containing lower biliary levels of TGF-β1)[2] displayed decreased fibrosis mRNA expression and increased cellular senescence compared to HHSteCs treated with cholangiocyte supernatant from Mdr2$^{-/-}$ mice.

Changes in ductular reaction in response to cholestatic liver injury are modulated by a number of neuroendocrine/gastrointestinal factors such as gastrin, histamine, angiogenic factors (e.g., VEGF-A), neurotransmitters, melatonin, sex hormones and Sct[5, 28, 29]. Among these neuroendocrine factors, Sct (that exerts its effects by selective interaction with basolateral SR expressed only by cholangiocytes)[12] plays a key role in the autocrine modulation of biliary damage/proliferation/homeostasis in addition to the paracrine regulation of liver inflammation and fibrosis[2, 5, 7–9, 31]. For example, we have previously shown that: (i) Sct increases ductular reaction both by autocrine/paracrine pathways through upregulation of cAMP-dependent protein kinase A signaling as well as microRNA 125b-dependent VEGF-A expression[9, 28, 30]; and (ii) knockout of the Sct/SR axis reduces biliary hyperplasia as well as liver fibrosis by a paracrine mechanism involving microRNA 125b-dependent decrease of biliary TGF-β1 secretion and reduced VEGF-A expression[2, 9]. Ingenuity Pathway Analysis indicated that the Sct/SR axis is a major upstream regulator of the pathway networks under our experimental conditions, may be suggesting a central role of Sct in regulating liver senescence, angiogenesis and fibrosis. However, our previous studies have limitation because we did not evaluate the potential role of the Sct/SR/microRNA 125b/TGF-β1/VEGF-A axis on the modulation of cellular senescence that may affect both the senescence of cholangiocytes (by an autocrine loop) as well as the senescence of HSCs by a paracrine mechanism mediated by the release of SASP (e.g., in addition to TGF-β1, interleukin-6 (IL-6), IL-8, CCL2, p16/21, SA-β-gal, PAI-1 and substance P)[16–18, 31, 32], biliary SASP that play a key role in the activation of HSCs and liver fibrosis[16, 33]. Supporting this finding, a recent *in vitro* study in the human cholangiocyte line, MMNK-1, has identified by microarray analysis differentially regulated genes in response to lysophosphatidylcholine, which included IL-6/8, TGF-β1 and PAI-1[31]. Parallel to this line of research, we have not only demonstrated that TGF-β1, induces the activation of HSCs through decreased cellular senescence by a paracrine mechanism, but also provided novel evidence that TGF-β1 increases biliary senescence by an autocrine loop, thus further increasing the paracrine activation of HSCs by cholangiocytes. Moreover, supporting the key role of TGF-β1 in modulating biliary homeostasis and liver fibrosis, Mdr2$^{-/-}$ mice treated with the SR antagonist (Sec 5–27) displayed reduced biliary mass and HSCs activation, which correlates with decreased TGF-β1/TGF-β1 receptor axis expression[2]. The observation that attenuated liver fibrosis is associated with decreased senescence of cholangiocytes

(associated with reduced Sct-dependent TGF-β1 expression/secretion) is consistent with the finding by Moncsek et al.[33], who demonstrated that senescent cholangiocytes promote the development of liver fibrosis by secretion of Bcl-XL, which is a key survival factor for several senescent cell types. Inhibition of Bcl-XL in $Mdr2^{-/-}$ mice depletes senescent cholangiocytes and reduces liver fibrosis.

Since we have previously demonstrated that Sct increases liver fibrosis by: (i) downregulation of microRNA 125b leading to upregulation of VEGF-A; and (ii) stimulation of biliary TGF-β1 secretion, we performed *in vitro* experiments to demonstrate that: **a.** Sct-stimulation of TGF-β1 biliary expression/secretion in IMCLs is mediated by microRNA 125b; and **b.** upregulation of VEGF-A in IMCLs (which also increases proliferation and cellular senescence of cholangiocytes by an autocrine loop)[25] is mediated by the Sct-modulation of TGF-β1 expression. In support of this concept, microRNA 125b has been shown to play an important role in the regulation of TGF-β1/Smads signaling. For example, microRNA 125b has been shown to be negatively correlated with TGF-β1/Smads signaling pathway in a model of peribiliary fibrosis caused by Clonorchis sinensis[34]. Furthermore, other studies have shown that the downstream targets of miRNA 125b include STAT3, IL-6 as well as TGF-β/Smads signaling[35, 36]. Also, microRNA 125b has been shown to potentiate early neural specification of human embryonic stem cells by a Smad4-dependent mechanism, since reduced microRNA 125b expression leads to upregulation of Smad4[36]. Taken together, our findings support the hypothesis that the Sct/microRNA 125b/TGF-β1 axis plays a key role in the autocrine modulation of biliary senescence as well as the paracrine regulation of liver fibrosis through decreased HSCs senescence. Since we have shown that Sct increases biliary proliferation by microRNA 125b-dependent increase in VEGF-A, we performed experiments that demonstrated that r-VEGF-A increases (in addition to biliary proliferation)[25] fibrosis and senescence mRNA expression of IMCLs but increases fibrosis and decreases cellular senescence in HHSteCs. Although VEGF has been shown to: (i) decrease the expression of the senescent genes, p16/p21, in human dermal microvascular endothelial cells; and (ii) to increase biliary proliferation[25] and periductular fibrosis[37] and fibrogenesis of HSCs[27], no information exists regarding the effect of VEGF-A on biliary and HSC senescence. On this basis, our study provides novel information that VEGF-A is an important SASP that increases biliary senescence (that subsequently activates HSCs by a paracrine pathway) as well as directly HSC fibrogenic activity through decreased HSC senescence. The data introduce the key concept that the Sct/microRNA 125b/TGF-β1/VEGF-A axis is an important mediator of biliary and HSC fibrogenic activity through different changes in biliary (autocrine loop) and HSC (paracrine loop) senescence. Since HSCs secrete VEGF[38], we have to also consider in our models the possibility that changes of VEGF-A signaling affects the fibrogenic activity and cellular senescence of HSCs by an autocrine pathway.

However, one of the unsolved questions of this study is the mechanism by which the Sct/SR/microRNA 125b/TGF-β1/VEGF-A axis regulates the differential changes of senescence in cholangiocytes and HSCs. We postulate that this difference may be explained in terms of the heterogeneity of the biliary epithelium[39], as the Sct/SR axis may target different sized cholangiocytes that may respond differentially to liver injury. We speculate that a subset of

large cholangiocytes may lose the ability to proliferate and undergo cellular senescence and subsequently interact with nearby undamaged small and large cholangiocytes inducing damage/senescence of these cells. However, additional studies are required to isolate and characterize these different subsets of cholangiocytes in order to pinpoint the specific subpopulations of cholangiocytes undergoing senescence.

A proposed working model for our study is depicted in Figure 7. We have identified that long-term depletion of SR in genetically altered $SR^{-/-}/Mdr2^{-/-}$ mice has a significant impact on ductular reaction/fibrosis (by an autocrine loop involving the Sct/TGF-β1 axis), cellular senescence and fibrogenic activity of HSCs by a paracrine mechanism. Modulation of the Sct/SR/TGF-β1 axis may be a key therapeutic target in the treatment of cholangiopathies including PSC.

Supplementary Material

Refer to Web version on PubMed Central for supplementary material.

Acknowledgments

This work was supported partly by the Dr. Nicholas C. Hightower Centennial Chair of Gastroenterology from Scott & White, a VA Research Career Scientist Award, a VA Merit award to Dr. Alpini (5I01BX000574), a VA Merit Award (5I01BX002192) to Dr. Glaser, a VA Merit Award (1I01BX001724) to Dr. Meng from the United States and a VA Merit Award (1I01BX003031) to Dr. Francis, Department of Veterans Affairs Biomedical Laboratory Research and Development Service, by University of Rome “La Sapienza” to Dr. Onori, and the NIH grants DK058411, DK110035, DK076898, DK108959 and DK062975 to Drs. Alpini, Meng and Glaser. Dr. C Wu is supported by grants from American Diabetes Association (1-17-IBS-145) and the NIH grant DK095862.

Abbreviations

α-SMA	alpha smooth muscle actin
BDL	bile duct ligated
CCL2	C-C motif chemokine ligand 2
CD31	platelet endothelial cell adhesion molecule 1
CK-19	cytokeratin-19
Col1a1	collagen, type I, alpha 1
FN-1	fibronectin-1
GAPDH	glyceraldehyde-3-phosphate dehydrogenase
HHSteCs	human hepatic stellate cell lines
HSCs	hepatic stellate cells
IBDM	intrahepatic bile duct mass
IL-6	interleukin 6
IMCLS	immortalized murine biliary cell lines

IPA	Ingenuity pathway analysis
LCM	laser capture microdissection
PAI-1	plasminogen activator inhibitor-1
PCNA	proliferating cellular nuclear antigen
PSC	primary sclerosing cholangitis
***q*PCR**	real-time PCR
p16	cyclin-dependent kinase inhibitor 2A
SA-β-gal	senescence associated beta galactosidase
Sct	secretin
SR	secretin receptor
TGF-β	transforming growth factor beta-1
TNF-α	tumor necrosis factor alpha
VEGF	vascular endothelial growth factor
WT	wild-type

References

1. Kanno N, LeSage G, Glaser S, et al. Regulation of cholangiocyte bicarbonate secretion. Am J Physiol Gastrointest Liver Physiol. 2001; 281:G612–625. [PubMed: 11518673]
2. Wu N, Meng F, Invernizzi P, et al. The secretin/secretin receptor axis modulates liver fibrosis through changes in transforming growth factor-beta1 biliary secretion in mice. Hepatology. 2016; 64:865–879. [PubMed: 27115285]
3. Lazaridis KN, LaRusso NF. The Cholangiopathies. Mayo Clin Proc. 2015; 90:791–800. [PubMed: 25957621]
4. Lazaridis KN, Strazzabosco M, LaRusso NF. The cholangiopathies: disorders of biliary epithelia. Gastroenterology. 2004; 127:1565–1577. [PubMed: 15521023]
5. Hall C, Sato K, Wu N, et al. Regulators of Cholangiocyte Proliferation. Gene Expr. 2017; 17:155–171. [PubMed: 27412505]
6. Chung BK, Karlsen TH, Folseraas T. Cholangiocytes in the pathogenesis of primary sclerosing cholangitis and development of cholangiocarcinoma. Biochim Biophys Acta. 2017 Aug 25. pii: S0925-4439(17)30302-2. [Epub ahead of print]. doi: 10.1016/j.bbadis.2017.08.020
7. Alpini G, Lenzi R, Sarkozi L, et al. Biliary physiology in rats with bile ductular cell hyperplasia. Evidence for a secretory function of proliferated bile ductules. JCI. 1988; 81:569–578. [PubMed: 2448343]
8. Glaser S, Lam IP, Franchitto A, et al. Knockout of secretin receptor reduces large cholangiocyte hyperplasia in mice with extrahepatic cholestasis induced by bile duct ligation. Hepatology. 2010; 52:204–214. [PubMed: 20578263]
9. Glaser S, Meng F, Han Y, et al. Secretin stimulates biliary cell proliferation by regulating expression of microRNA 125b and microRNA let7a in mice. Gastroenterology. 2014; 146:1795–1808 e1712. [PubMed: 24583060]

10. Alpini G, Glaser S, Robertson W, et al. Large but not small intrahepatic bile ducts are involved in secretin-regulated ductal bile secretion. Am J Physiol Gastrointest Liver Physiol. 1997; 272:G1064–1074.
11. Alpini G, Roberts S, Kuntz SM, et al. Morphological, molecular, and functional heterogeneity of cholangiocytes from normal rat liver. Gastroenterology. 1996; 110:1636–1643. [PubMed: 8613073]
12. Alpini G, Ulrich CD 2nd, Phillips JO, et al. Upregulation of secretin receptor gene expression in rat cholangiocytes after bile duct ligation. Am J Physiol Gastrointest Liver Physiol. 1994; 266:G922–928.
13. Zhang Z, Yao Z, Zhao S, et al. Interaction between autophagy and senescence is required for dihydroartemisinin to alleviate liver fibrosis. Cell Death Dis. 2017 Jun 15.8(6):e2886.doi: 10.1038/cddis.2017.255 [PubMed: 28617435]
14. Rapisarda V, Borghesan M, Miguela V, et al. Integrin Beta 3 Regulates Cellular Senescence by Activating the TGF-beta Pathway. Cell Rep. 2017; 18:2480–2493. [PubMed: 28273461]
15. Tabibian JH, Trussoni CE, O'Hara SP, et al. Characterization of cultured cholangiocytes isolated from livers of patients with primary sclerosing cholangitis. Lab Invest. 2014; 94:1126–1133. [PubMed: 25046437]
16. Meng L, Quezada M, Levine P, et al. Functional role of cellular senescence in biliary injury. Am J Pathol. 2015; 185:602–609. [PubMed: 25619959]
17. Loarca L, De Assuncao TM, Jalan-Sakrikar N, et al. Development and characterization of cholangioids from normal and diseased human cholangiocytes as an in vitro model to study primary sclerosing cholangitis. Lab Invest. 2017; 97:1385–1396. [PubMed: 28892096]
18. Wan Y, Meng F, Wu N, et al. Substance P increases liver fibrosis by differential changes in senescence of cholangiocytes and hepatic stellate cells. Hepatology. 2017; 66:528–541. [PubMed: 28256736]
19. Ikenaga N, Liu SB, Sverdlov DY, et al. A new Mdr2($^{-/-}$) mouse model of sclerosing cholangitis with rapid fibrosis progression, early-onset portal hypertension, and liver cancer. Am J Pathol. 2015; 185:325–334. [PubMed: 25478810]
20. Baghdasaryan A, Claudel T, Gumhold J, et al. Dual farnesoid X receptor/TGR5 agonist INT-767 reduces liver injury in the Mdr2$^{-/-}$ (Abcb4$^{-/-}$) mouse cholangiopathy model by promoting biliary HCO(−)(3) output. Hepatology. 2011; 54:1303–1312. [PubMed: 22006858]
21. Puche JE, Lee YA, Jiao J, et al. A novel murine model to deplete hepatic stellate cells uncovers their role in amplifying liver damage in mice. Hepatology. 2013; 57:339–350. [PubMed: 22961591]
22. Han Y, Onori P, Meng F, et al. Prolonged exposure of cholestatic rats to complete dark inhibits biliary hyperplasia and liver fibrosis. Am J Physiol Gastrointest Liver Physiol. 2014; 307:G894–904. [PubMed: 25214401]
23. Kennedy LL, Meng F, Venter JK, et al. Knockout of microRNA-21 reduces biliary hyperplasia and liver fibrosis in cholestatic bile duct ligated mice. Lab Invest. 2016; 96:1256–1267. [PubMed: 27775690]
24. Ren XF, Mu LP, Jiang YS, et al. LY2109761 inhibits metastasis and enhances chemosensitivity in osteosarcoma MG-63 cells. Eur Rev Med Pharmacol Sci. 2015; 19:1182–1190. [PubMed: 25912577]
25. Gaudio E, Barbaro B, Alvaro D, et al. Vascular endothelial growth factor stimulates rat cholangiocyte proliferation via an autocrine mechanism. Gastroenterology. 2006; 130:1270–1282. [PubMed: 16618418]
26. Sato K, Meng F, Venter J, et al. The role of the secretin/secretin receptor axis in inflammatory cholangiocyte communication via extracellular vesicles. Sci Rep. 2017; 7:11183. [PubMed: 28894209]
27. Yoshiji H, Kuriyama S, Yoshii J, et al. Vascular endothelial growth factor and receptor interaction is a prerequisite for murine hepatic fibrogenesis. Gut. 2003; 52:1347–1354. [PubMed: 12912869]
28. Alvaro D, Mancino MG, Glaser S, et al. Proliferating cholangiocytes: a neuroendocrine compartment in the diseased liver. Gastroenterology. 2007; 132:415–431. [PubMed: 17241889]

29. Maroni L, Haibo B, Ray D, et al. Functional and structural features of cholangiocytes in health and disease. Cell Mol Gastroenterol Hepatol. 2015; 1:368–380. [PubMed: 26273695]

30. Guerrier M, Attili F, Alpini G, et al. Prolonged administration of secretin to normal rats increases biliary proliferation and secretin-induced ductal secretory activity. Hepatobiliary Surg Nutr. 2014; 3:118–125. [PubMed: 25019073]

31. Shimizu R, Kanno K, Sugiyama A, et al. Cholangiocyte senescence caused by lysophosphatidylcholine as a potential implication in carcinogenesis. J Hepatobiliary Pancreat Sci. 2015; 22:675–682. [PubMed: 25921542]

32. Tabibian JH, O'Hara SP, Splinter PL, et al. Cholangiocyte senescence by way of N-ras activation is a characteristic of primary sclerosing cholangitis. Hepatology. 2014; 59:2263–2275. [PubMed: 24390753]

33. Moncsek A, Al-Suraih MS, Trussoni CE, et al. Targeting senescent cholangiocytes and activated fibroblasts with Bcl-xL inhibitors ameliorates fibrosis in Mdr2($^{-/-}$) mice. Hepatology. 2017; 67:247–259. [PubMed: 28802066]

34. Yan C, Shen LP, Ma R, et al. Characterization and identification of differentially expressed microRNAs during the process of the peribiliary fibrosis induced by Clonorchis sinensis. Infect Genet Evol. 2016; 43:321–328. [PubMed: 27267304]

35. Yin H, Sun Y, Wang X, et al. Progress on the relationship between miR-125 family and tumorigenesis. Exp Cell Res. 2015; 339:252–260. [PubMed: 26407906]

36. Boissart C, Nissan X, Giraud-Triboult K, et al. miR-125 potentiates early neural specification of human embryonic stem cells. Development. 2012; 139:1247–1257. [PubMed: 22357933]

37. Gaudio E, Barbaro B, Alvaro D, et al. Administration of r-VEGF-A prevents hepatic artery ligation-induced bile duct damage in bile duct ligated rats. Am J Physiol Gastrointest Liver Physiol. 2006; 291:G307–317. [PubMed: 16574985]

38. Zhao Y, Wang Y, Wang Q, et al. Hepatic stellate cells produce vascular endothelial growth factor via phospho-p44/42 mitogen-activated protein kinase/cyclooxygenase-2 pathway. Mol Cell Biochem. 2012; 359:217–223. [PubMed: 21863308]

39. Han Y, Glaser S, Meng F, et al. Recent advances in the morphological and functional heterogeneity of the biliary epithelium. Exp Biol Med. 2013; 238:549–565.

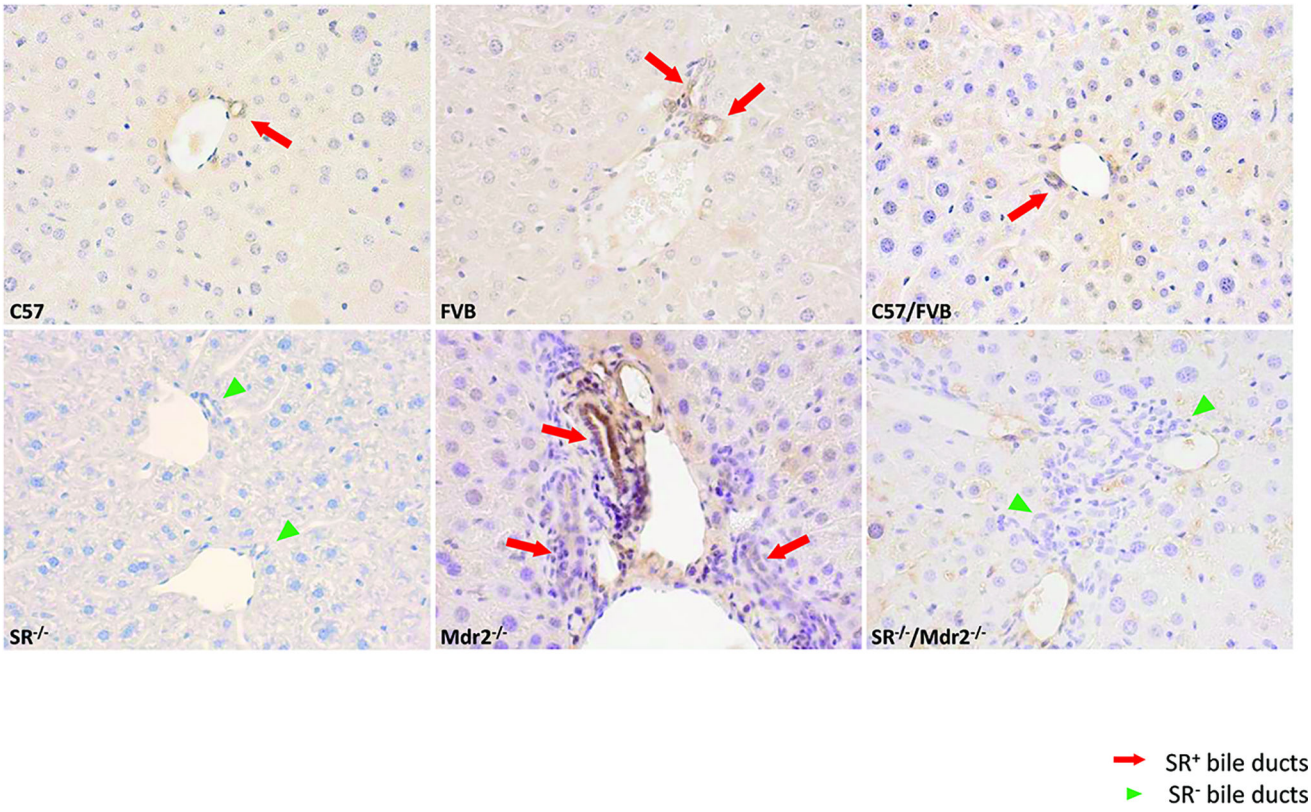

Figure 1.

Expression of SR in liver sections. Immunohistochemistry for SR shows that $Mdr2^{-/-}$ mice have higher immunoreactivity for SR (red arrows depicting bile ducts) compared to WT mice. No immunoreactivity was observed for SR in $SR^{-/-}$ and $SR^{-/-}/Mdr2^{-/-}$ mice (green arrowheads). Original magn., 40×.

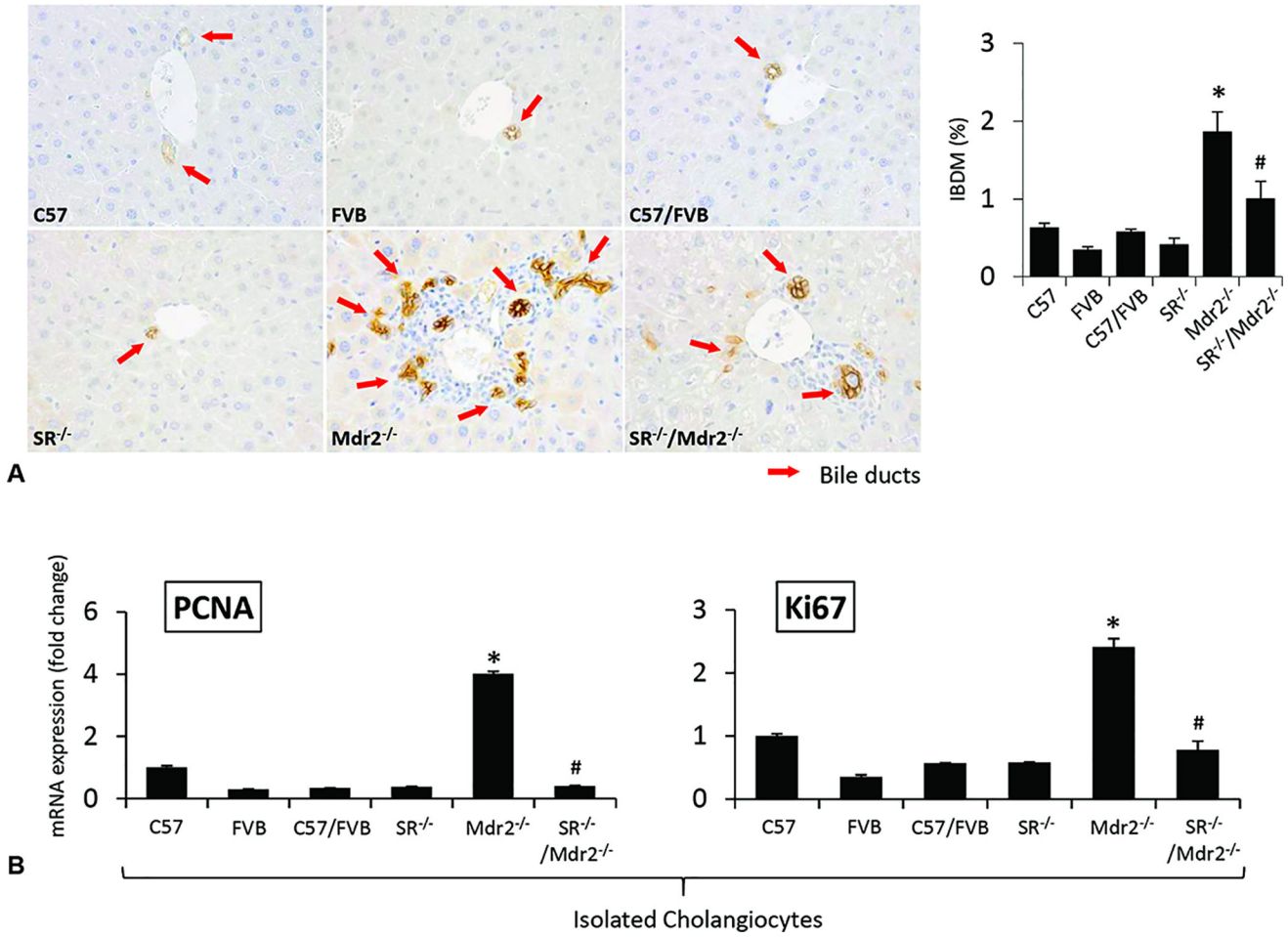

Figure 2.

[**A–B**] Measurement of ductular reaction. [**A**] There was increased IBDM (red arrows) in Mdr2$^{-/-}$ mice compared to WT mice, which was reduced in SR$^{-/-}$/Mdr2$^{-/-}$ mice compared to Mdr2$^{-/-}$ mice; no significant changes in IBDM were noted in SR$^{-/-}$ compared to WT mice. Original magn., 40×. [**B**] There was increased mRNA expression of PCNA and Ki67 in cholangiocytes from Mdr2$^{-/-}$ mice, which was decreased in SR$^{-/-}$/Mdr2$^{-/-}$ compared to Mdr2$^{-/-}$ mice. Data are mean ± SEM of n=3 from a cumulative preparation of cholangiocytes from 8 mice. *p<0.05 versus FVB mice; $^{\#}$p<0.05 versus Mdr2$^{-/-}$ mice.

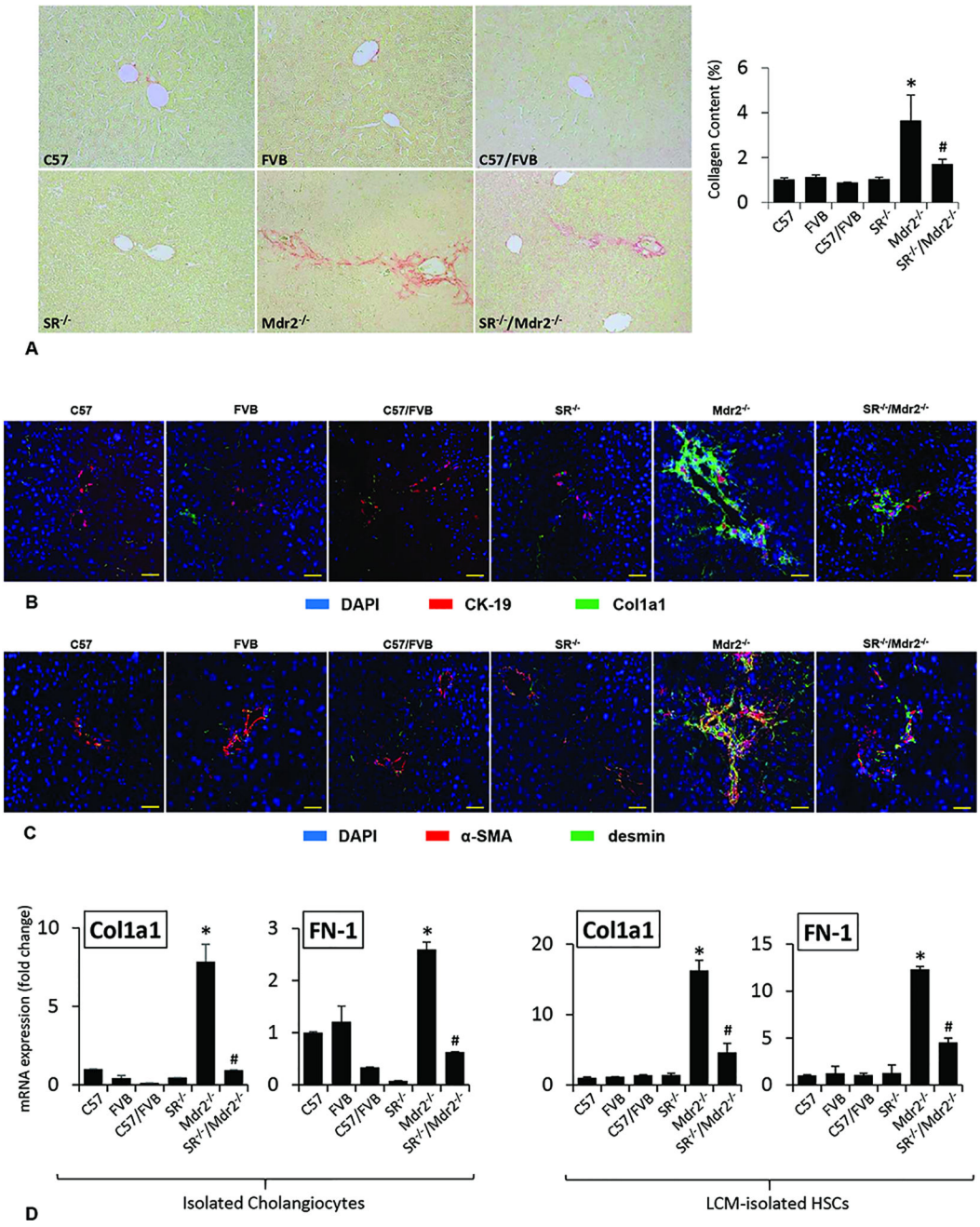

Figure 3.

[**A**] Measurement of collagen deposition in liver sections. There was enhanced collagen deposition in Mdr2$^{-/-}$ mice compared to WT mice, which was significantly decreased in SR$^{-/-}$/Mdr2$^{-/-}$ compared to Mdr2$^{-/-}$ mice. Orig. magn., ×20. [**B–C**] By immunofluorescence in liver sections, there was enhanced immunoreactivity for Col1a1 (green color, costained with CK-19 in red) in Mdr2$^{-/-}$ (compared to WT mice), which was reduced in SR$^{-/-}$/Mdr2$^{-/-}$ compared to Mdr2$^{-/-}$ mice. There was enhanced co-localization of α-SMA and desmin (α-SMA in green color, costained with desmin in red) in HSCs from Mdr2$^{-/-}$ compared to WT that was decreased in SR$^{-/-}$/Mdr2$^{-/-}$ compared to Mdr2$^{-/-}$ mice. Scale bar

= 100 μm. [**D**] There was enhanced expression of Col1a1 and FN-1 in isolated cholangiocytes and HSCs from $Mdr2^{-/-}$ mice compared to the corresponding WT mice, increase that was significantly reduced in $SR^{-/-}/Mdr2^{-/-}$ mice compared to $Mdr2^{-/-}$ mice. Data are mean ± SEM of n=3 from one cumulative preparation of cholangiocytes from 8 mice, and 3 preparations of LCM-isolated HSCs from 3 mice. *$p<0.05$ vs. FVB mice; $^{\#}p<0.05$ vs. $Mdr2^{-/-}$ mice.

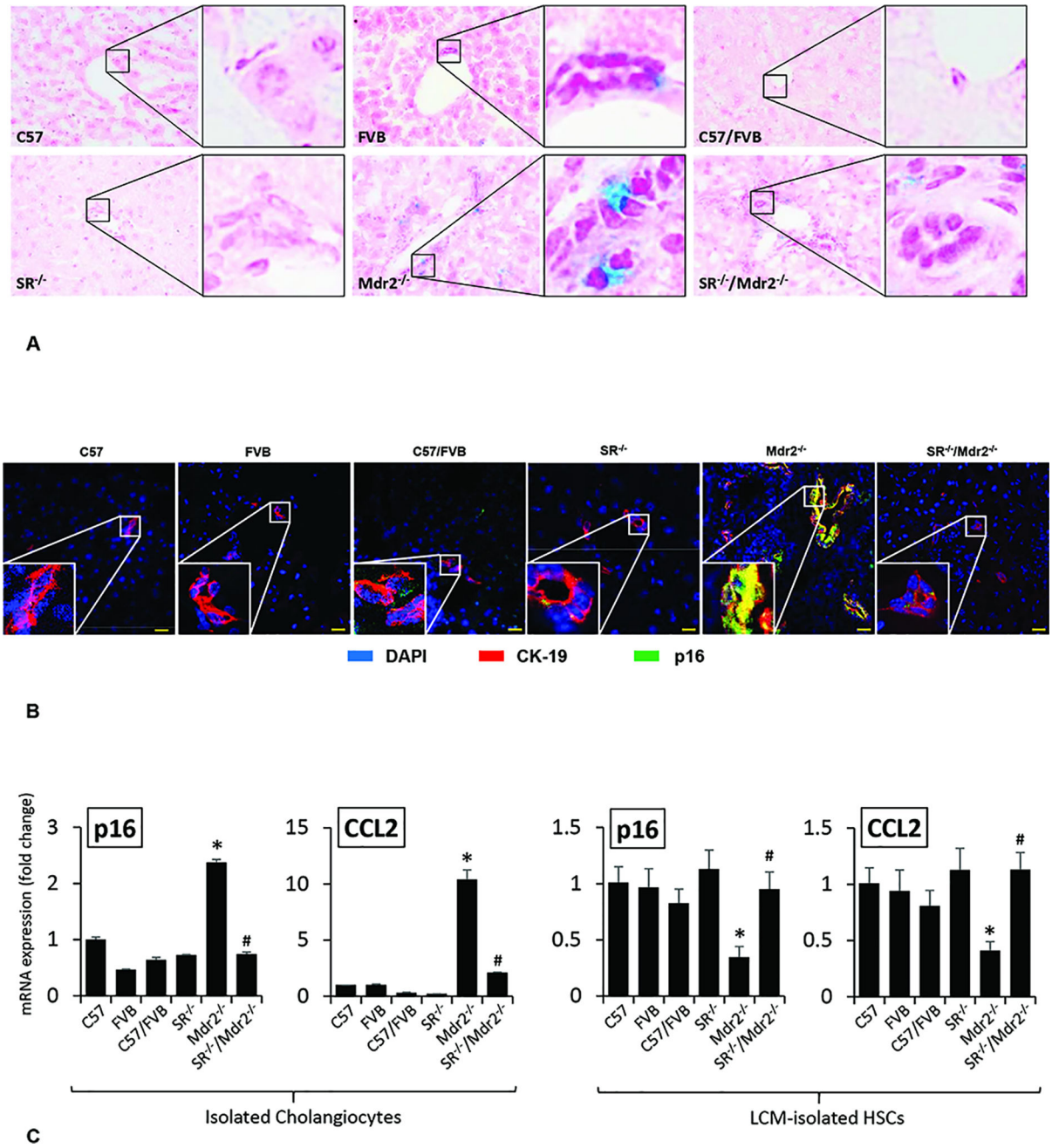

Figure 4.

[**A**] Measurement of cellular senescence in liver sections by SA-β-gal staining in liver sections (orig. magn., ×40), there was enhanced cellular senescence in liver sections from $Mdr2^{-/-}$ mice compared to the respective WT mice, which was decreased in $SR^{-/-}/Mdr2^{-/-}$ mice compared to $Mdr2^{-/-}$ mice. [**B**] There was enhanced immunoreactivity for p16 (green, co-stained with CK-19, red) in liver sections from $Mdr2^{-/-}$ mice compared to corresponding WT mice, which was reduced in $SR^{-/-}/Mdr2^{-/-}$ compared to $Mdr2^{-/-}$ mice; nuclei are stained with DAPI. Scale bar = 20 μm. [**C**] There was enhanced expression of p16 and CCL2 in cholangiocytes from $Mdr2^{-/-}$ mice compared to relative WT mice but decreased in

cholangiocytes from $SR^{-/-}/Mdr2^{-/-}$ compared to $Mdr2^{-/-}$ mice. The expression of p16 and CCL2 was significantly decreased in HSCs from $Mdr2^{-/-}$ compared to relative WT mice, changes that returned to values similar to that of WT group in $SR^{-/-}/Mdr2^{-/-}$ mice. Data are mean ± SEM of n=3 from one cumulative preparation of cholangiocytes from 8 mice, and 3 preparations of LCM-isolated HSCs from 3 mice. *$p<0.05$ vs. FVB mice; $^{\#}p<0.05$ vs. $Mdr2^{-/-}$ mice.

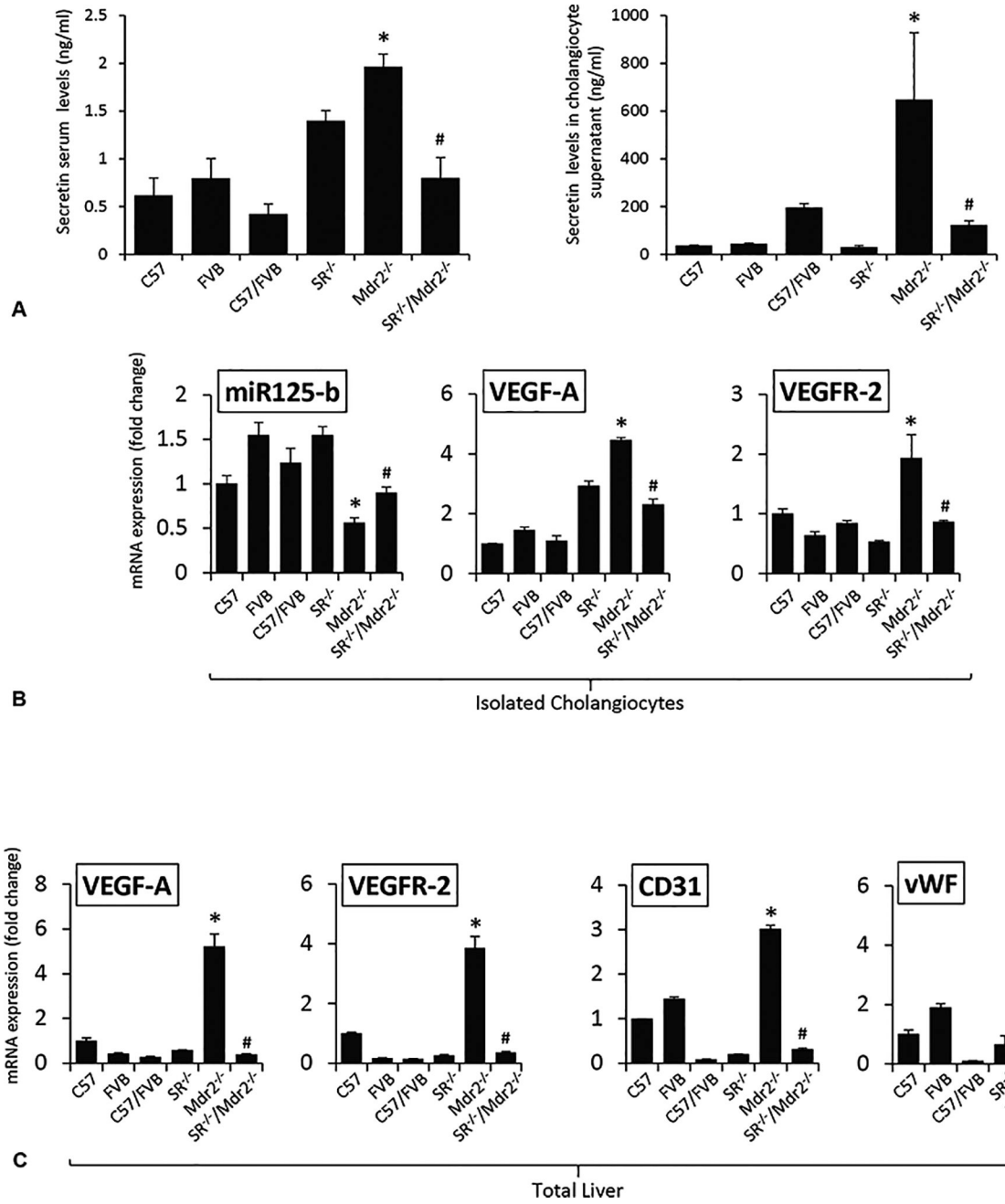

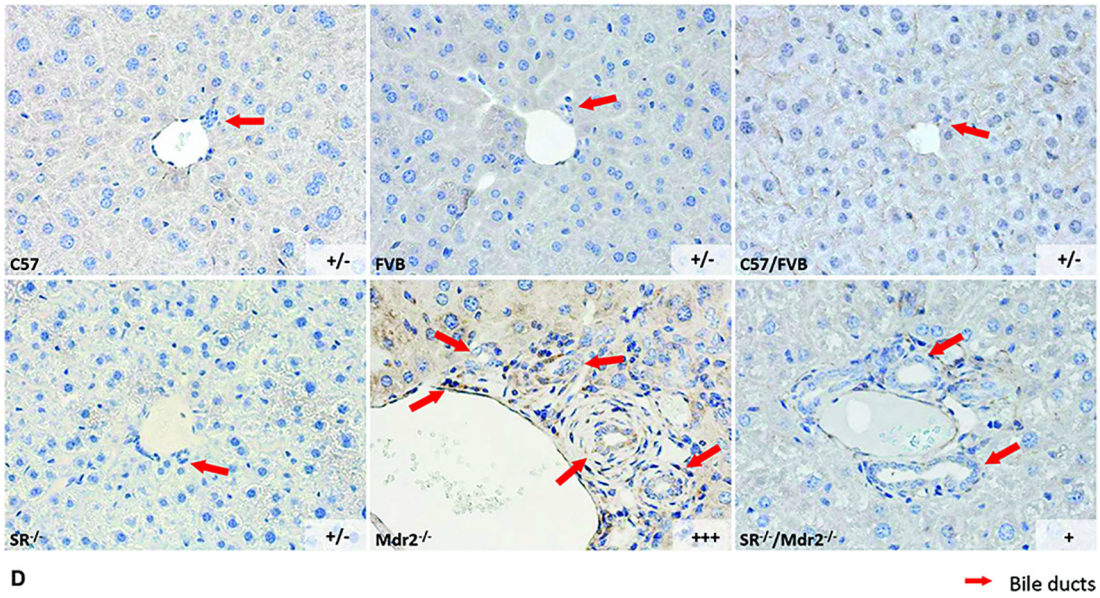

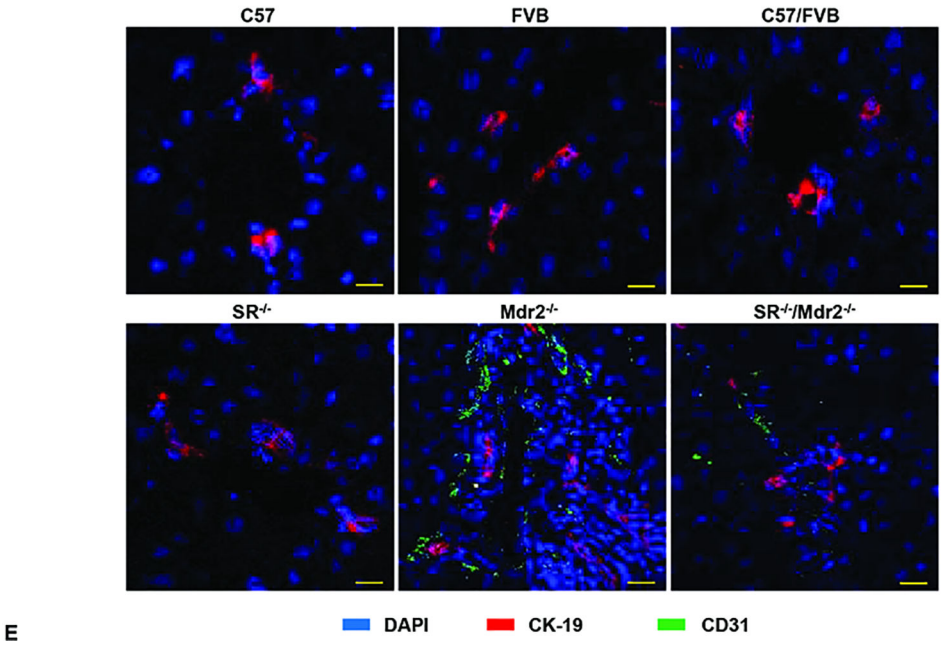

Figure 5.

[**A**] Both Sct levels in serum and cholangiocyte supernatant were increased in Mdr2$^{-/-}$ mice compared to relative WT mice, which was decreased in SR$^{-/-}$/Mdr2$^{-/-}$ mice compared to Mdr2$^{-/-}$ mice. *p<0.05 vs. FVB mice; $^{\#}$p<0.05 vs. Mdr2$^{-/-}$ mice. Data are mean ± SEM of n=3 from 9 mice. [**B–C**] There was enhanced expression microRNA 125b in cholangiocytes, VEGF-A and VEGFR-2 in both cholangiocytes and total liver, as well as CD31 and vWF in total liver from Mdr2$^{-/-}$ mice compared to the corresponding WT mice, expression that returned to values similar to that of normal WT group in SR$^{-/-}$/Mdr2$^{-/-}$ mice. Data are mean ± SEM of n=3 from one cumulative preparation of cholangiocytes from 8 mice, and 3

total liver samples from 3 mice. *p<0.05 vs. FVB mice; #p<0.05 vs. Mdr2$^{-/-}$ mice. [**D**] There was enhanced immunoreactivity for VEGF-A in liver sections from Mdr2$^{-/-}$ mice compared to relative WT mice, which was reduced in SR$^{-/-}$/Mdr2$^{-/-}$ mice compared to Mdr2$^{-/-}$ mice; orig. magn., ×40. [**E**] There was enhanced immunoreactivity for CD-31 (green color, costained with CK-19 in red) in liver sections from Mdr2$^{-/-}$ mice compared to relative WT mice, which was reduced in SR$^{-/-}$/Mdr2$^{-/-}$ mice compared to Mdr2$^{-/-}$ mice; Scale bar = 100 μm.

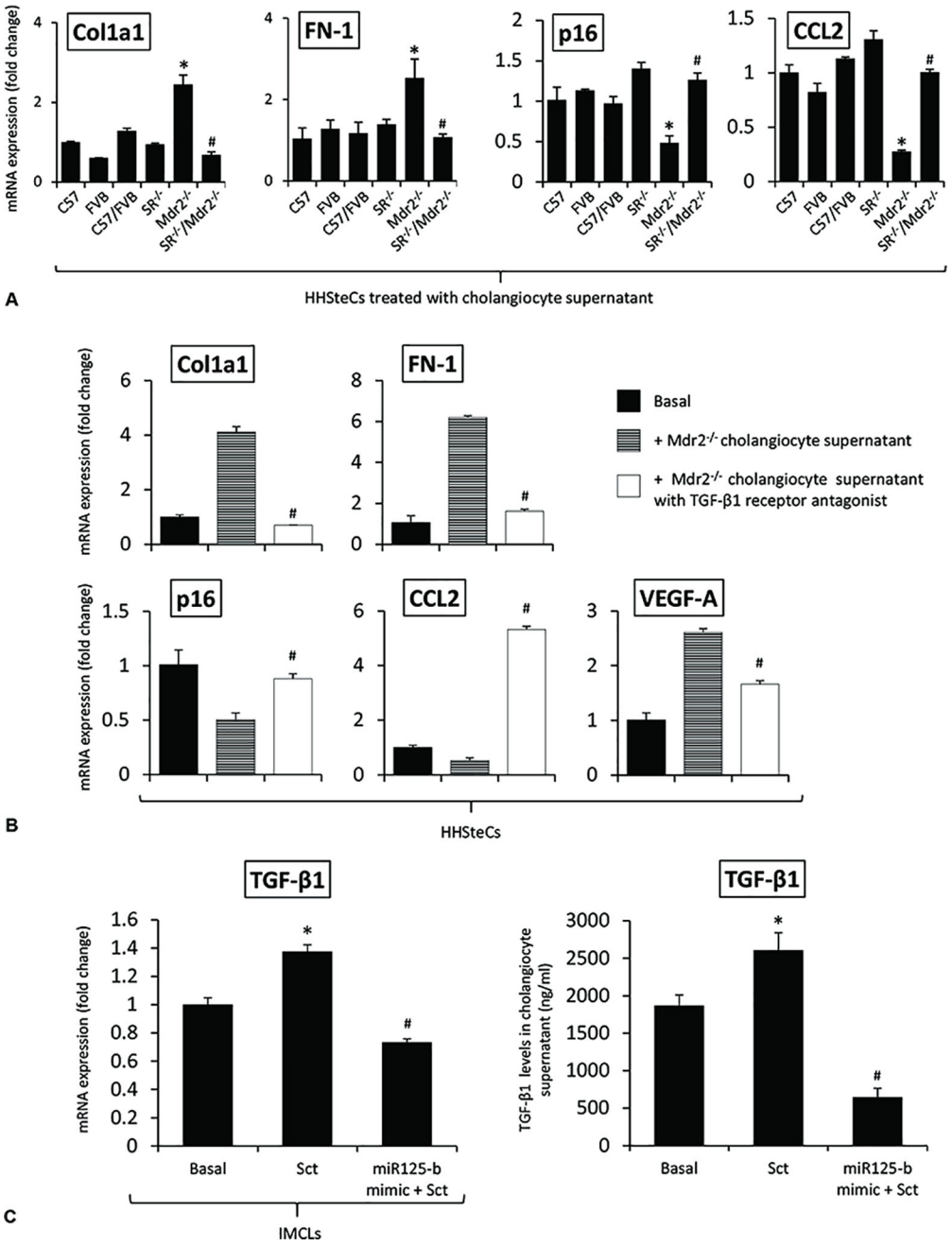

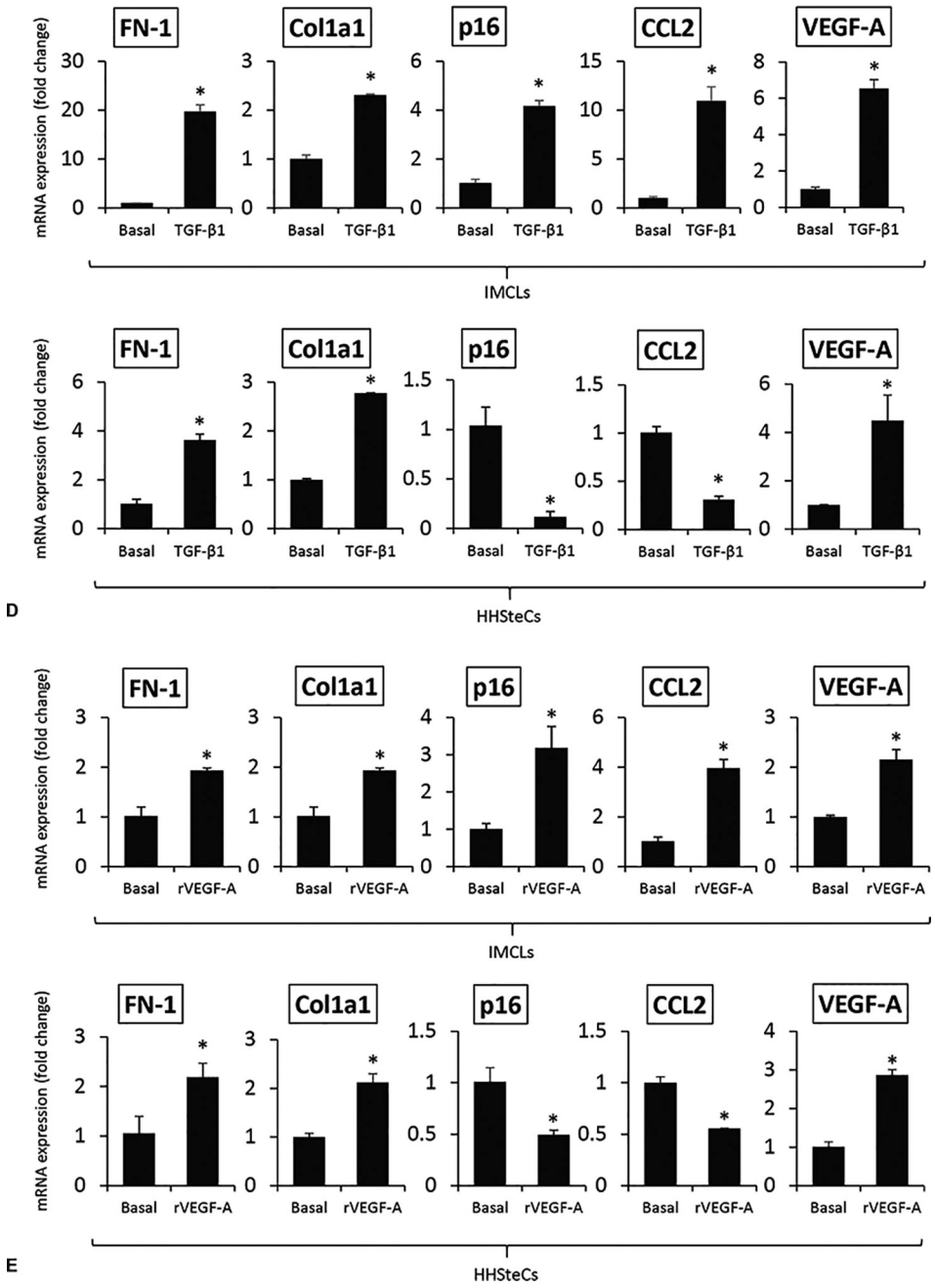

Figure 6.

[**A–B**] There was increased expression of fibrosis but decreased senescence gene expression in HHSteCs treated with cholangiocyte supernatant from Mdr2$^{-/-}$ mice compared to HHSteCs treated with supernatant from WT, effects that were reversed when HHSteCs were treated with cholangiocyte supernatant from SR$^{-/-}$/Mdr2$^{-/-}$. These effects were reversed when HHSteCs were preincubated with LY2109761 before treatment with the cholangiocyte supernatants from Mdr2$^{-/-}$ mice. No effects were observed with WT cholangiocyte supernatant. Data are mean ± SEM of 3 different evaluations. *p<0.05 vs. HHSteCs treated with cholangiocyte supernatant from FVB mice. $^{\#}$p<0.05 vs. HHSteCs treated with

cholangiocyte supernatant from Mdr2$^{-/-}$ mice. [**C**] Sct increased TGF-β1 mRNA expression of IMCLs and TGF-β1 levels in IMCLs supernatant, increases that were prevented by preincubation of IMCLs with a microRNA 125b precursor before treatment with Sct. *p<0.05 vs. Basal. $^{\#}$p<0.05 vs. Sct. [**D–E**] Treatment of: (i) IMCLs with TGF-β1 and r-VEGF-A, respectively, increased the expression of VEGF-A, fibrosis and senescence genes; and (ii) HHSteCs with TGF-β1 and r-VEGF-A, respectively, increased the expression of VEGF-A, fibrosis but decreased senescence genes in HHSteCs. *p<0.05 vs. basal value.

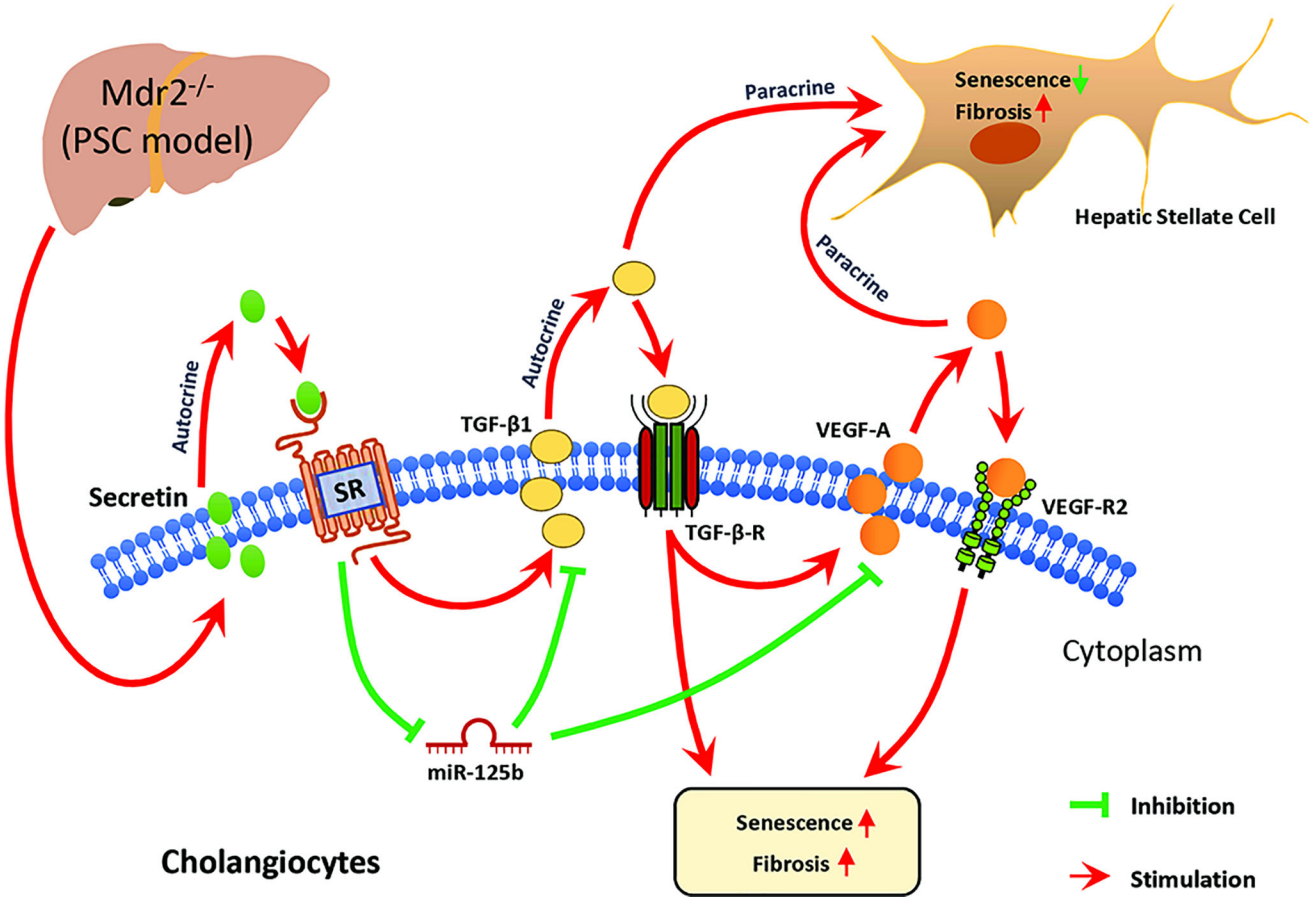

Figure 7.

In the Mdr2$^{-/-}$ mouse model, there is activation of the Sct/SR axis that increases microRNA 125b-dependent TGF-β1 biliary secretion that: (i) increases cholangiocyte senescence by an autocrine mechanism; and (ii) triggers liver fibrosis by a paracrine loop. The increase in TGF-β1 biliary secretion (mediated by the Sct/SR/microRNA 125b axis) leads to enhanced VEGF-A expression, which subsequently increases cholangiocyte senescence (by an autocrine loop) and increases fibrogenic activity but decreases cellular senescence of HSCs by a paracrine loop.

Table 1

Evaluation of liver and body weight, and liver to body weight ratio, serum chemistry and levels of TGF-β1 in serum and cholangiocyte supernatant.

Parameters	C57	FVB	C57/FVB	SR$^{-/-}$	Mdr2$^{-/-}$	SR$^{-/-}$/Mdr2$^{-/-}$
Liver weight (gm)	1.7±0.3 n=34	1.6±0.1 n=13	1.6±0.1 n=12	1.6±0.4 n=15	2.6±0.1 * n=15	2.2±0.1 n=11
Body weight (gm)	26.0±0.5 n=34	30.0±0.5 n=13	31.1±1.4 n=12	32.0 ± 1.5 n=15	30.6±0.4 n=15	30.6±1.1 n=11
Liver to body weight ratio (%)	6.4±0.2 n=34	5.4±0.1 n=13	5.2±0.3 n=12	5.7±0.2 n=15	8.5±0.3 * n=15	7.2±0.1 # n=11
SGPT (Units/L)	326.3±32.6 n=4	131.3±16.6 n=4	124.3±11.9 n=4	321.5±68.4 n=4	1153.5±55.6 * n=4	794.5±21.9 # n=4
SGOT (Units/L)	485.0±53.5 n=4	431.3±25.9 n=4	570±89.8 n=4	427.5±174.3 n=4	1710.3±216.8 * n=4	893.8±102.8 # n=4
ALP (Units/L)	<45±5.0 n=4	<50±0.0 n=4	<56.5±6.5 n=4	<47.25±2.8 n=4	342.5±27.2 * n=4	237.0±17.5 # n=4
TGF-β1 levels in serum (pg/ml)	276.9±36.3 n=4	78.7±4.7 n=4	118.5±10.2 n=4	69.4±0.8 n=4	7970.7±304.8 * n=4	1617.5±132.3 # n=4
TGF-β1 levels in cholangiocyte supernatant (ng/ml)	4.0±0.5 n=4	0.5±0.3 n=4	1.3±0.5 n=4	24.7±1.2 n=4	764.5±30.0 * n=4	216.9±10.6 # n=4

*P<0.05 vs. FVB mice;

#P<0.05 vs. Mdr2$^{-/-}$ mice.